

Supporting Information

Dramatically Accelerated Selective Oxygen-Atom- Transfer by a Nonheme Iron(IV)-Oxo Complex: Tuning of the First and Second Coordination Spheres

Leland R. Widger,[†] Casey G. Davies,^{||} Tzuhsiung Yang,[†] Maxime A. Siegler,[†] Oliver Troeppner,[§] Guy N. L. Jameson,^{*,||} Ivana Ivanović-Burmazović,[§] and David P. Goldberg^{*,†}

[†]Department of Chemistry, The Johns Hopkins University, 3400 North Charles Street
Baltimore, Maryland 21218, United States

^{||}Department of Chemistry & MacDiarmid Institute for Advanced Materials and Nanotechnology
University of Otago, PO Box 56, Dunedin 9054, New Zealand

[§]Department of Chemistry and Pharmacy, University of Erlangen-Nuremberg, 91058 Erlangen, Germany

I. Experimental

General Procedures. All reagents were purchased from commercial vendors, and used without further purification unless otherwise noted. Dichloromethane and diethyl ether were purified via a Pure-Solv Solvent Purification System from Innovative Technology, Inc. Methanol and acetonitrile were distilled over CaH₂. All solvents were degassed by repeated cycles of freeze-pump-thaw and stored in an N₂-filled drybox. Iron-57 metal (95.63%) was purchased from Cambridge Isotope Laboratories, Inc.; tetrafluoroboric acid (48% w/w) was purchased from Aldrich. Reactions requiring inert atmosphere were performed in an N₂-filled drybox or with standard Schlenk techniques. Iodosobenzene,¹ 3-((2-(hydroxymethyl)phenyl)thio)propanenitrile,² di(2-pyridyl)methanamine,³ and *N*-(6-(bromomethyl)-2-pyridyl)pivalamide⁴ were prepared according to reported procedures.

Physical Methods. UV-visible spectra were recorded on a Varian Cary 50 spectrophotometer. NMR spectra were recorded on a Bruker Avance 400 MHz FT-NMR spectrometer at 25 °C. Elemental analysis was performed by Atlantic Microlab Inc., Norcross, GA. Electron paramagnetic resonance (EPR) spectra were obtained on a Bruker EMX EPR spectrometer controlled with a Bruker ER 041 X G microwave bridge at 15 K. The EPR spectrometer was equipped with a continuous-flow liquid He cryostat and an ITC503 temperature controller made by Oxford Instruments, Inc. Mössbauer spectra were recorded on a spectrometer from SEE Co. (Science Engineering & Education Co., MN) equipped with a closed cycle refrigerator system from Janis Research Co. and SHI (Sumitomo Heavy Industries Ltd.). MS measurements were performed on a UHR-ToF Bruker Daltonik (Bremen, Germany) maXis, which was coupled to a Bruker cryospray unit, an ESI-ToF MS capable of resolution of at least 40,000 FWHM. Detection was in positive-ion mode and the source voltage was 4.5 kV. The flow rates were 200 µL/hour. The dry-gas temperature (N₂) was held at -40 °C and the spray-gas temperature was held at -35 °C. The machine was calibrated prior to every experiment via direct infusion of the Agilent ESI-ToF low concentration tuning mixture, which provided an *m/z* range of singly charged peaks up to 2700 Da in both ion modes.

Computational Methods. Complexes $[\text{Fe}^{\text{II}}(\text{N3PyamideSR})]^{2+}$ (**1**) and $[\text{Fe}^{\text{IV}}(\text{O})(\text{N3PyamideSR})]^{2+}$ (**2**) in various spin states were investigated by computational methods: (**1**) in the singlet and (**2**) in the triplet and quintet spin states. Calculations utilized density functional theory (DFT) as implemented in the Gaussian-09 and Orca-2.6.35 program packages.^{5,6} The geometry of **1** was fully optimized (without constraints) with 6-31G(d) basis set^{7,8,9} implemented on all atoms with DFT at the unrestricted hybrid density functional level B3LYP. Single point energies with zero-point energy corrections were calculated using these optimized geometries. Calculations were performed on the $\text{Fe}^{\text{IV}}(\text{O})$ complex, **2** in the Orca-3.0.0 program package. The geometry of $[\text{Fe}^{\text{IV}}(\text{O})(\text{N3PyamideSR})]^{2+}$ (**2**) was calculated for both the triplet and quintet spin states. The geometries were optimized (without constraints) with LANLDZ on the iron and 6-31G on the rest of the atoms, including the auxiliary basis sets def2-SVP/J and def2-SVP/K for the RIJCOSX approximation,^{10,11} with DFT at the unrestricted hybrid density functional level B3LYP. Optimized structures of **2** were employed as the starting point for single point calculations using LANLTDZ+ on the iron and 6-311+G* on the rest of the atoms. Calculated Mössbauer parameters were obtained from the optimized geometries using the Orca-2.6.35 and Orca-3.0.0 program packages. These calculations used the B3LYP method in conjunction with the CP(PPP)¹² basis set on Fe and TZVP¹³ basis set on all remaining atoms. The quadrupole splitting (ΔE_Q) was obtained directly, and the isomer shift (δ) was obtained from the calculated spin density at the iron nucleus $\rho_0(\text{Fe})$ using a previously determined calibration curve.¹⁴

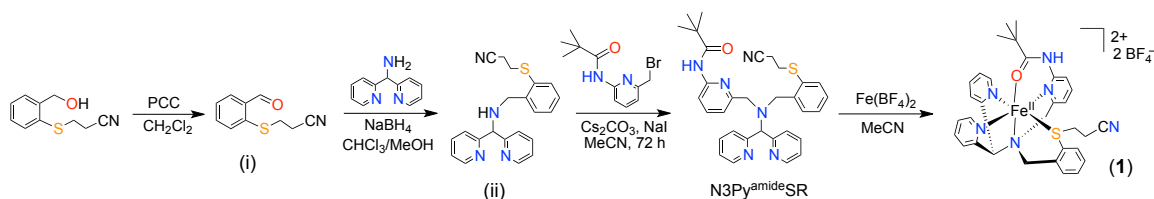


Figure S1. Synthesis of **1**.

Aldehyde (i). An amount of 3-((2-(hydroxymethyl)phenyl)thio)propanenitrile (5.7 g, 29.5 mmol) was dissolved in CH_2Cl_2 (100 mL) and added to a stirring suspension of

pyridinium chlorochromate (9.5 g, 44.1 mmol) in CH_2Cl_2 (300 mL). The mixture was stirred for several hours before being diluted with Et_2O , filtered through Celite and concentrated. The crude product was purified by column chromatography on silica (EtOAc/hexanes) to give the desired product as a white solid (5.1 g, 90%). ^1H NMR (CDCl_3): δ 10.31 (s, 1 H), 7.82 (m, 1 H), 7.53 (m, 1 H), 7.41 (d, $J = 8.1$ Hz, 1H), 7.35 (t, $J = 7.5$ Hz, 1H), 3.18 (t, $J = 7.2$ Hz, 2 H) 2.67 (t, $J = 7.2$ Hz, 2 H); ^{13}C NMR (CDCl_3): δ 191.6, 138.5, 134.6, 132.8, 129.7, 127.3, 126.6, 117.9, 29.5, 18.0.

Secondary amine (ii). Aldehyde (i) (2.73 g, 14.3 mmol) and di(2-pyridyl)methanamine (2.64 g, 14.3 mmol) were dissolved in a 1:1 mixture of $\text{CHCl}_3/\text{MeOH}$ (80 mL). A small amount of 4 Å molecular sieves was added and the reaction was allowed to stir overnight under Ar atmosphere. An amount of NaBH_4 (540 mg, 14.3 mmol) was added in small portions and the reaction mixture was allowed to stir for 3 h before being filtered through Celite and concentrated. The resulting residue was dissolved in CHCl_3 , washed with water, dried and concentrated. Purification by column chromatography on neutral alumina (EtOAc/hexanes) gave the desired product as a yellow solid (2.06 g, 40%). ^1H NMR (CDCl_3): δ 8.59 (m, 2 H), 7.65 (m, 2 H), 7.48 – 7.41 (m, 4 H), 7.29 – 7.25 (m, 2 H), 7.17 (m, 2 H), 5.15 (s, 1 H), 3.96 (s, 2 H), 3.10 (t, $J=7.3$ Hz, 2 H), 2.55 (t, $J=7.3$ Hz, 2 H); ^{13}C NMR (CDCl_3): δ 161.7, 149.5, 142.3, 136.9, 132.9, 132.4, 130.5, 128.4, 128.3, 122.7, 122.5, 118.4, 69.0, 50.35, 30.64, 18.41.

N3Py^{amide}SR. Secondary amine (ii) (1.23 g, 3.4 mmol) was dissolved in MeCN (100 mL) before Cs_2CO_3 (1.7 g, 5.2 mmol), *N*-(6-(bromomethyl)-2-pyridyl)pivalamide (925 mg, 3.4 mmol), and NaI (767 mg, 5.1 mmol) were added. The mixture was stirred under Ar atmosphere for 24 h before additional portions of Cs_2CO_3 (1.7 g, 5.2 mmol), and NaI (767 mg, 5.1 mmol) were added. After stirring for an additional 48 h, the crude reaction mixture was filtered through Celite and concentrated. The residue was dissolved in CHCl_3 , washed with H_2O , dried and concentrated. Purification by column chromatography on neutral alumina (EtOAc/hexanes) gave the desired product as a pale yellow solid (1.1 g, 60%). ^1H NMR (CDCl_3): δ 8.56 (m, 2 H), 8.01 (m, 1 H), 7.97 (br, 1 H), 7.78 (dd, $J = 7.6, 1.5$ Hz, 1 H), 7.67 - 7.55 (m, 5 H), 7.30 (dd, $J = 7.6, 1.3$ Hz, 1 H),

7.24 – 7.12 (m, 5 H), 5.34 (s, 1 H), 4.03 (s, 2 H), 3.86 (s, 2 H), 3.00 (t, $J = 7.3$ Hz, 2 H) 2.48 (t, $J = 7.3$ Hz, 2 H) 1.32 (s, 9 H); ^{13}C NMR (CDCl_3): δ 177.2, 160.2, 158.2, 150.8, 149.4, 141.2, 138.7, 136.4, 132.5, 131.4, 129.9, 127.9, 127.7, 124.1, 122.4, 118.8, 118.2, 112.0, 72.5, 56.8, 53.9, 39.9, 36.9, 30.0, 27.7, 18.2.

[Fe^{II}(N3Py^{amide}SR)](BF₄)₂•CH₃CN (1**•CH₃CN).** An amount of the free ligand (N3Py^{amide}SR) (1.0 g, 1.82 mmol) was dissolved in MeCN and Fe(BF₄)₂•6H₂O (615 mg, 1.82 mmol) was added. The yellow solution immediately changed to an orange color, and was then stirred for 2 h. The mixture was concentrated to a residue, which was dissolved in a minimum amount of MeCN. Vapor diffusion of Et₂O into this solution gave complex **1** as dark red crystals suitable for X-ray diffraction (1.25 g, 88%). UV-Vis (MeCN): 350 nm (4700 M⁻¹cm⁻¹), 450 nm (6000 M⁻¹cm⁻¹); ^1H NMR (CD_3CN , 25 °C): δ 68.3, 45.0, 36.6, 29.8, 29.0, 27.6, 26.9, 23.1, 16.9, 15.6, 11.7, 10.4, 9.6, 7.3, 7.0, 6.6, 6.3, 4.3, 3.3, 1.0, -13.5.; *Anal. Calc.* for [**1**] (C₃₂H₃₄B₂F₈FeN₆OS): C, 49.26; H, 4.39; N, 10.77. Found: C, 48.59; H, 4.37; N, 10.63. m/z (ESI-ToF, -40 °C) = 303.0917 [**1** – 2BF₄]²⁺.

Generation of [Fe^{IV}(O)(N3Py^{amide}SR)]²⁺ (2**) for characterization by UV-vis spectroscopy.** An amount of **1** (0.8 mg, 1.0 μmol) was dissolved in MeCN (5.0 mL), and cooled to -40 °C in a flask equipped with a submersible UV-vis probe. A stock solution of PhIO in MeOH was freshly prepared, and then 0.1 mL of this PhIO solution (0.12 μmol , 1.2 equiv) was added. The reaction mixture changed in color from orange to yellow over 30 min. Monitoring the reaction by UV-vis spectroscopy revealed the disappearance of the characteristic peaks for **1** (350, 450 nm), and the appearance of a new peak at 750 nm, corresponding to **2**.

[Fe^{II}(Cl)(N3Py^{amide}SR)](BF₄) (3**).** An amount of the ligand (**iii**) (12.3 mg, 0.016 mmol) was dissolved in 2 mL of MeCN and FeCl₂ (2.2 mg, 0.017 mmol) was added. The mixture was allowed to stir for 1 h, and NaBF₄ (1.9 mg, 0.017 mmol) was added. After stirring for an additional 2 h the solution was filtered through Celite, and vapor diffusion of Et₂O gave **3** as yellow crystals suitable for X-ray diffraction (8.3 mg, 67%). ^1H NMR (CD_3CN): δ 63.3, 56.4, 41.4, 35.3, 28.9, 26.1, 25.2, 16.4, 14.2, 12.5, 12.0, 8.2, 7.9, 7.7,

7.3, 6.0, 3.6, 3.4, 1.2, 0.9, -1.6; UV-vis: $\lambda_{\max} = 358 \text{ nm}$, $\epsilon = 5000 \text{ M}^{-1} \text{ cm}^{-1}$; *Anal. Calc.* for **3** ($\text{C}_{32}\text{H}_{34}\text{B}_2\text{ClF}_8\text{FeN}_6\text{OS}$): C, 47.12; H, 4.20; N, 10.30. Found: C, 47.61; H, 4.30; N, 10.04. m/z (LDI-MS) = 641.0 [**3** – BF_4]⁺.

[$\text{Fe}^{\text{II}}(\text{N3Py}^{\text{amide}}\text{S}(\text{O})\text{R})](\text{BF}_4)_2 \cdot 0.5 \text{ CH}_3\text{CN}$ (**4**•0.5 CH_3CN). An amount of **1** (9 mg, 0.012 mmol) was dissolved in MeCN (0.5 mL) and a solution of 75% *m*-CPBA (10.6 mg, 0.062 mmol) in MeCN (0.5 mL) was added. After stirring for 2 h, the green solution was concentrated and the residue was dissolved in CH_2Cl_2 and filtered through Celite. Successive vapor diffusion of Et_2O afforded X-ray quality crystals (4.7 mg, 49% yield). ^1H NMR (CD_3CN): δ 69.1, 67.0, 63.7, 60.7, 60.0, 58.9, 57.3, 56.8, 56.3, 55.9, 53.2, 46.0, 41.3, 33.6, 32.8, 31.8, 25.5, 22.3, 19.4, 18.7, 12.5, 10.0, 9.4, 9.0, 8.3, 8.1, 7.8, 7.7, 7.0, 6.5, 5.9, 5.4, 4.9, 4.0, 3.4, 3.0, 2.9, 2.5, 1.1; UV-vis: $\lambda_{\max} = 700 \text{ nm}$, $\epsilon = 1000 \text{ M}^{-1} \text{ cm}^{-1}$; *Anal. Calc.* for [**4**•0.5 CH_3CN •0.8 CH_2Cl_2] ($\text{C}_{33.8}\text{H}_{37.1}\text{B}_2\text{Cl}_{1.6}\text{F}_8\text{FeN}_{6.5}\text{O}_2\text{S}$): C, 45.89; H, 4.23; N, 10.29. Found: C, 46.02; H, 4.14; N, 9.96. m/z (LDI-MS) = 621.5 [**4** – H – 2BF_4]⁺. Note: Unresolved residual electron density, presumed to be disordered CH_2Cl_2 , was found in the crystal structure of **4** (see the X-ray crystallography section for further details). The elemental analysis was consistent with this assignment, in which a small amount of CH_2Cl_2 was added to obtain a good fit.

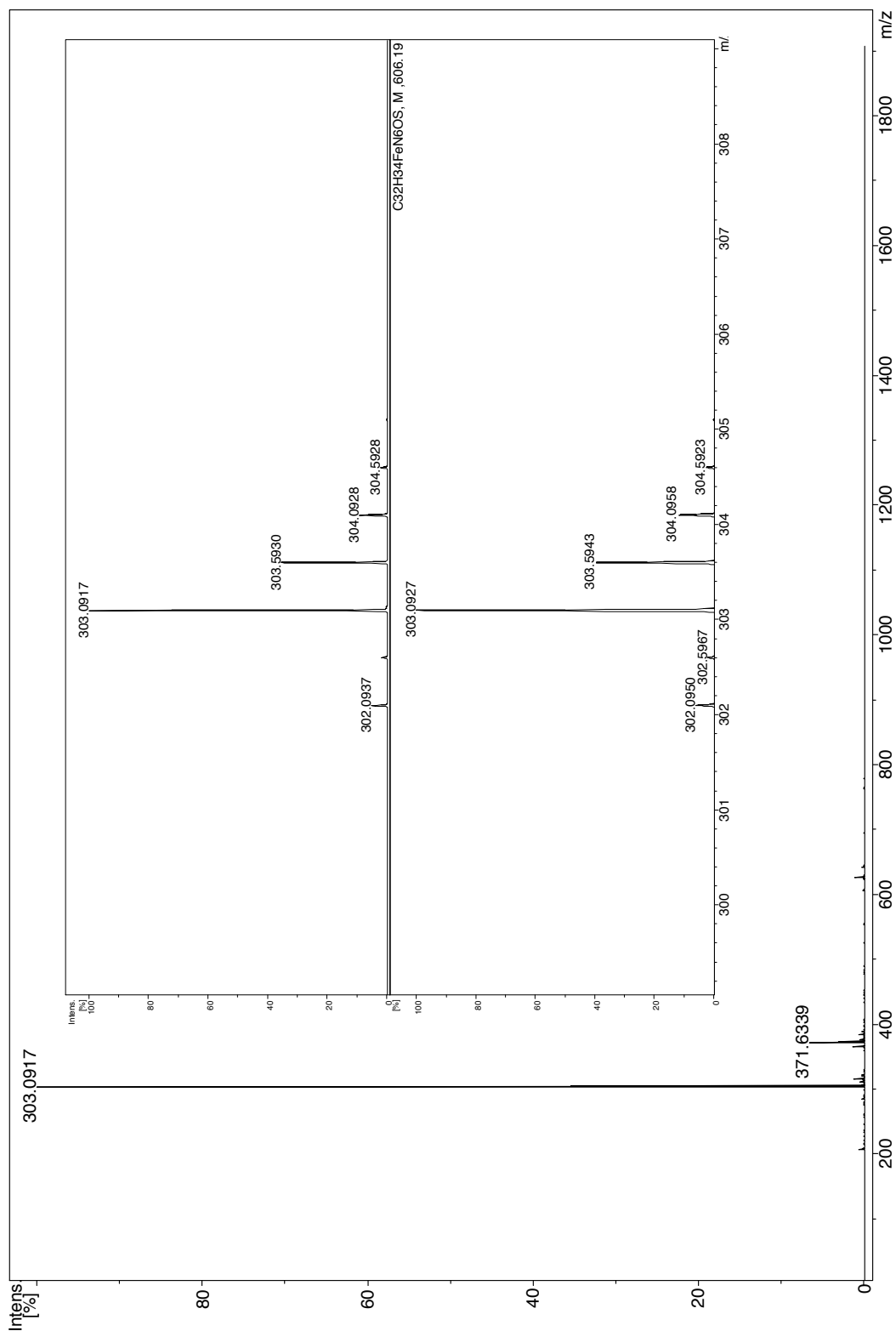


Figure S2. Cryo-UHR ESI-ToF mass spectrum of $[Fe^{II}(N3Py^{amide}SR)]^{2+}$ ($[1 - 2BF_4]^{2+}$) at $-40\text{ }^\circ\text{C}$ in MeCN/MeOH. Inset: top = experimental, bottom = simulated spectrum for $[C_{32}H_{34}FeN_6OS]^{2+}$.

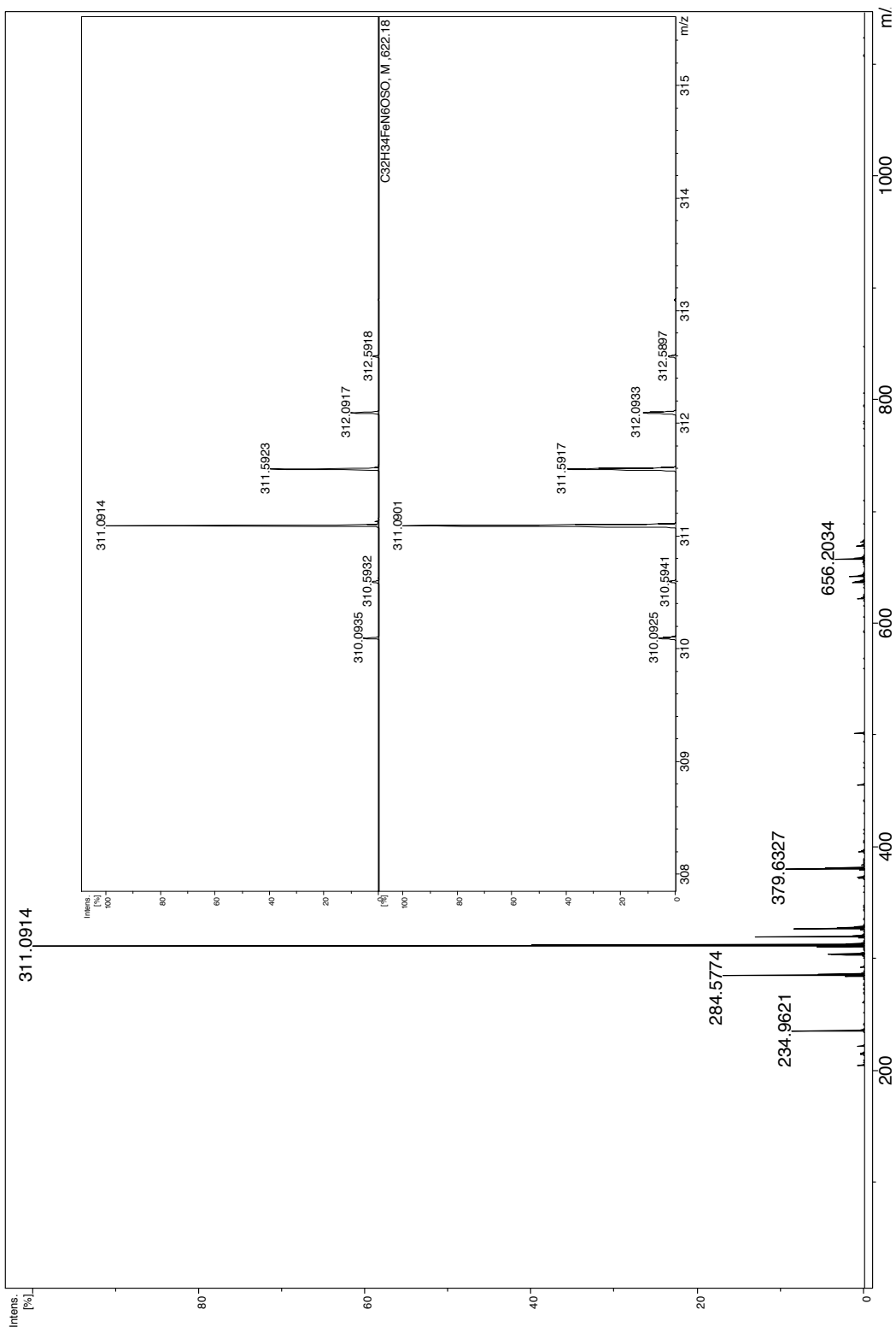


Figure S3. Cryo-UHR ESI-ToF mass spectrum of $[Fe^{IV}(O)(N3Py^{amide}SR)]^{2+}$ ($[2]^{2+}$) at -40 °C in MeCN/MeOH. Inset: top = experimental, bottom = simulated spectrum for $[C_{32}H_{34}FeN_6O_2S]^{2+}$.

II. X-ray Crystallography. All reflection intensities were measured at 110(2) K using a KM4/Xcalibur (detector: Sapphire3) with enhance graphite-monochromated Mo $K\alpha$ radiation ($\lambda = 0.71073 \text{ \AA}$) under the program CrysAlisPro (Versions 1.171.35.11 or 1.171.36.24 Agilent Technologies, 2011-2012). The program CrysAlisPro (Versions 1.171.35.11 or 1.171.36.24 Agilent Technologies, 2011-2012) was used to refine the cell dimensions. Data reduction was done using the program CrysAlisPro (Versions 1.171.35.11 or 1.171.36.24 Agilent Technologies, 2011-2012). The structures were solved with the program SHELXS-97 (Sheldrick, 2008), and refined on F^2 with SHELXL-97 (Sheldrick, 2008). Analytical numeric absorption corrections based on a multifaceted crystal model were applied using CrysAlisPro (Versions 1.171.35.11 or 1.171.36.24 Agilent Technologies, 2011-2012). The temperatures of the data collections were controlled using the system Cryojet (manufactured by Oxford Instruments). The H atoms (unless otherwise specified) were placed at calculated positions using the instructions AFIX 13, AFIX 23, AFIX 43 or AFIX 137 with isotropic displacement parameters having values 1.2 or 1.5 times U_{eq} of the attached C or N atoms. For the structure of **3**, the H atom attached to N6 was found from Fourier difference maps, and its atomic coordinates were refined freely.

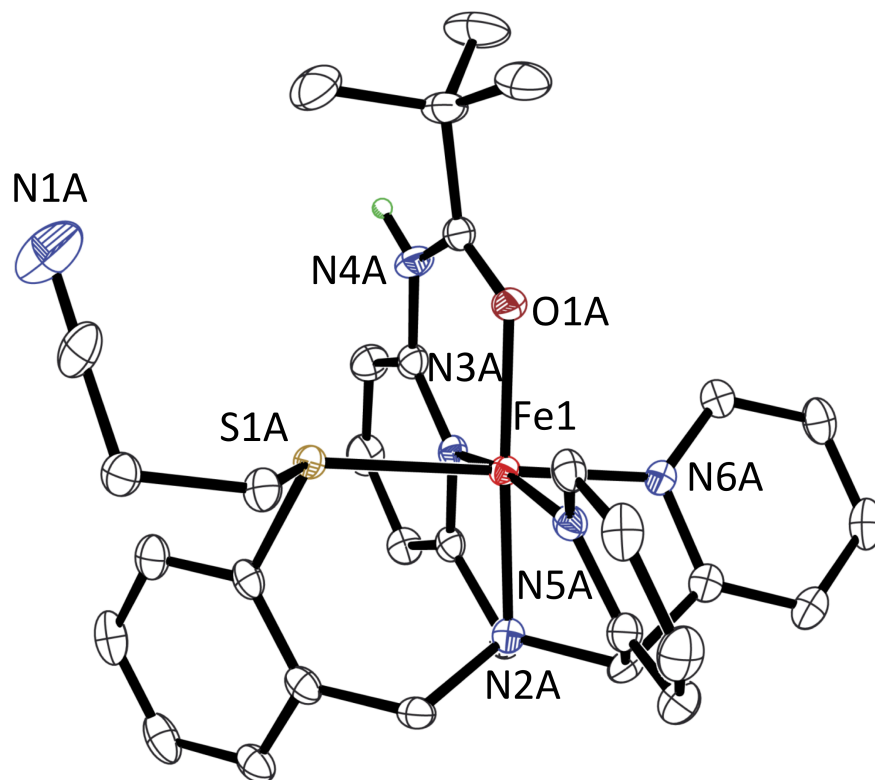


Figure S4. Displacement ellipsoid plots (50% probability level) of the dication of **1**. H-atoms and MeCN have been omitted for clarity, with the exception of the amide N-H.

Crystal Structure of 1•MeCN. Data were collected at 110 (2) K after the crystal had been flash-cooled from room temperature. Three crystallographically independent BF_4^- counterions are disordered. Two of the BF_4^- anions are found to be disordered over two orientations [occupancy factors for major components refine to 0.646(6) and 0.53(3)], while one is more severely disordered over 3 orientations [the three occupancy factors refine to 0.688(3), 0.214(3), and 0.099(2)].

Fw = 821.24, red thick lath, $0.39 \times 0.25 \times 0.15 \text{ mm}^3$, triclinic, $P-1$ (no. 2), $a = 12.7152(3)$, $b = 17.1863(3)$, $c = 17.3225(4) \text{ \AA}$, $\alpha = 89.9635(17)$, $\beta = 81.5135(19)$, $\gamma = 81.8096(18)^\circ$, $V = 3705.00(14) \text{ \AA}^3$, $Z = 4$, $D_x = 1.472 \text{ g cm}^{-3}$, $\mu = 0.543 \text{ mm}^{-1}$, abs. corr. range: 0.851–0.934. 45414 Reflections were measured up to a resolution of $(\sin \theta/\lambda)_{\text{max}} = 0.62 \text{ \AA}^{-1}$. 14972 Reflections were unique ($R_{\text{int}} = 0.0320$), of which 11595 were observed [$I > 2\sigma(I)$]. 1129 Parameters were refined using 579 restraints. $R1/wR2$ [$I > 2\sigma(I)$]:

0.0386/0.0995. $R1/wR2$ [all refl.]: 0.0552/0.1072. $S = 1.056$. Residual electron density found between -0.33 and $0.67 \text{ e } \text{\AA}^{-3}$.

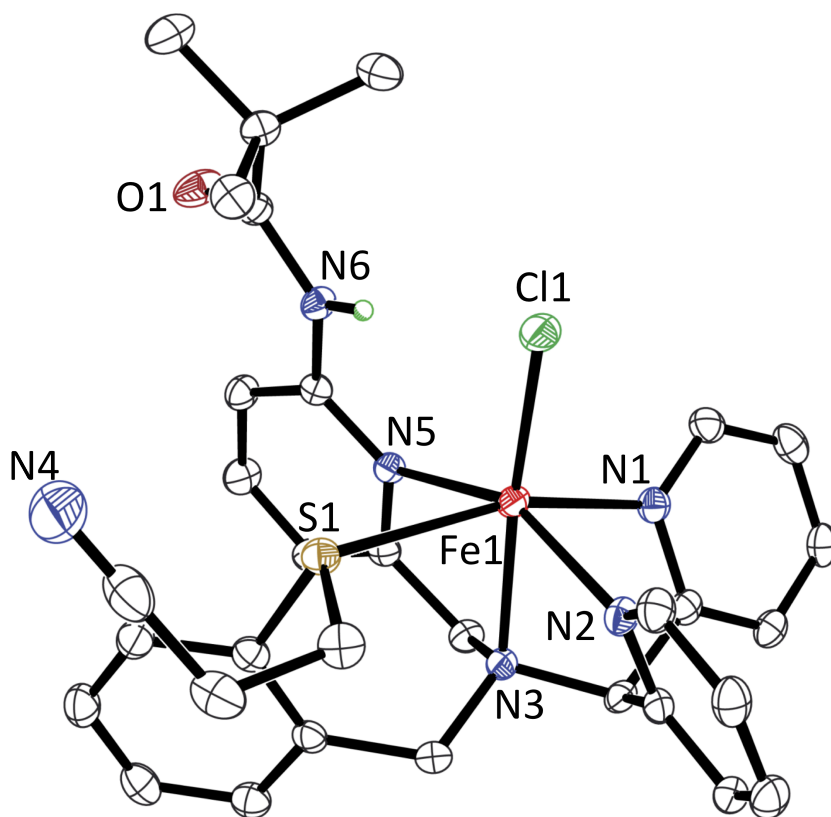


Figure S5. Displacement ellipsoid plots (50% probability level) of the cation of **3**. H-atoms have been omitted, with the exception of the amide N-H.

Crystal Structure of 3. The structure is ordered. The H atom attached to N6 was found from Fourier difference maps, and its atomic coordinates were refined freely. $F_w = 728.82$, irregular yellow block, $0.31 \times 0.24 \times 0.12 \text{ mm}^3$, monoclinic, $C2/c$ (no. 15), $a = 25.4707(3)$, $b = 9.98637(13)$, $c = 25.8674(3) \text{ \AA}$, $\beta = 94.8579(12)^\circ$, $V = 6555.99(14) \text{ \AA}^3$, $Z = 8$, $D_x = 1.477 \text{ g cm}^{-3}$, $\mu = 0.665 \text{ mm}^{-1}$, abs. corr. range: 0.870–0.947. 24531 Reflections were measured up to a resolution of $(\sin \theta/\lambda)_{\max} = 0.62 \text{ \AA}^{-1}$. 6622 Reflections were unique ($R_{\text{int}} = 0.0387$), of which 5537 were observed [$I > 2\sigma(I)$]. 431 Parameters were refined. $R1/wR2$ [$I > 2\sigma(I)$]: 0.0317/0.0777. $R1/wR2$ [all refl.]: 0.0418/0.0817. $S = 1.055$. Residual electron density found between -0.39 and $0.47 \text{ e } \text{\AA}^{-3}$.

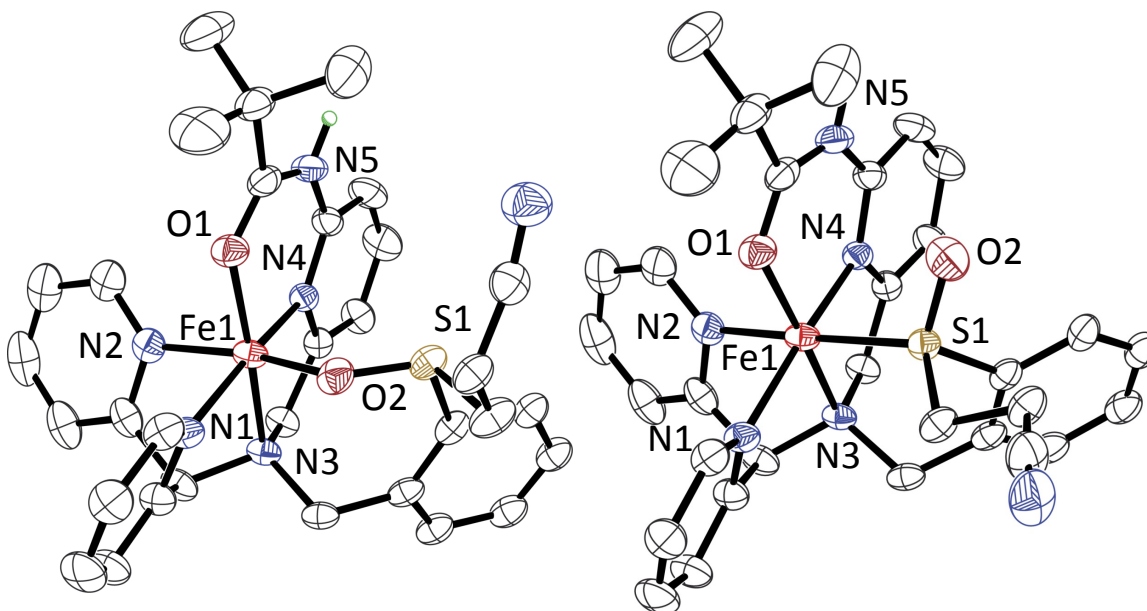


Figure S6. Displacement ellipsoid plots (50% probability level) of the O-bound (left) and S-bound (right) dications of **4**. H-atoms have been omitted, with the exception of the amide N-H.

Crystal Structure of 4. The structure is disordered because there are two possible modes of coordination on the Fe metal center in the crystal lattice. Some parts of the Fe complex are found to be disordered over 3 orientations. In two of the three orientations, the sixth coordination is achieved *via* S1, and occurs about 80% of the time. In the third orientation, the sixth coordination is achieved *via* O2. Both counterions are found to be disordered over two orientations [both occupancy factors for major components refine to 0.550(2)]. The lattice uncoordinated MeCN molecule is found to be disordered as the solvent molecule is found at a site of inversion symmetry. The crystal lattice also contains some CH₂Cl₂ solvent molecules disordered over another inversion center, but with probable occupancies lower than 1; their contributions were then taken out using the program SQUEEZE for the final refinement. All details of the SQUEEZE refinement are provided in the final CIF file.

Fw = 1633.42,* orange-red lath, 0.48 × 0.31 × 0.12 mm³, triclinic, *P*-1 (no. 2), *a* = 10.1678(3), *b* = 11.9592(3), *c* = 15.8456(3) Å, α = 92.0341(18), β = 96.166(2), γ = 108.703(2)°, *V* = 1809.49(8) Å³, *Z* = 1, *D*_x = 1.499 g cm⁻³,* μ = 0.557 mm⁻¹,* abs. corr.

range: 0.804–0.940. 29353 Reflections were measured up to a resolution of $(\sin \theta/\lambda)_{\max} = 0.62 \text{ \AA}^{-1}$. 7300 Reflections were unique ($R_{\text{int}} = 0.0347$), of which 6311 were observed [$I > 2\sigma(I)$]. 788 Parameters were refined with 1162 restraints. $R1/wR2$ [$I > 2\sigma(I)$]: 0.0475/0.1232. $R1/wR2$ [all refl.]: 0.0543/0.1271. $S = 1.050$. Residual electron density found between -0.75 and 0.58 e \AA^{-3} .

* excluding the contribution of the unresolved residual electron density

III. Mössbauer Spectroscopy

$^{57}\text{Fe}(\text{BF}_4)_2$. An amount of $^{57}\text{Fe}^0$ metal (50 mg, 0.9 mmol) was combined with aqueous HBF_4 (48% w/w, 2.0 equiv, 0.23 mL). The suspension was diluted with H_2O (0.27 mL) and heated to boiling on a sand bath. The solid slowly dissolved with heating, and care was taken to minimize solvent loss due to evaporation on the small scale. The pale blue solution was diluted to a final volume of 5.0 mL with MeCN. The final concentration of $^{57}\text{Fe}(\text{BF}_4)_2$, based on measured $^{57}\text{Fe}^0$, was 0.18 M.

$[^{57}\text{Fe}^{\text{II}}(\text{N3Py}^{\text{amide}}\text{SR})](\text{BF}_4)_2$. The $\text{N3Py}^{\text{amide}}\text{SR}$ ligand (**iii**) (5.0 mg, 0.01 mmol) was dissolved in a small amount of MeCN and freshly prepared $^{57}\text{Fe}(\text{BF}_4)_2$ (1.0 equiv, 56 μL of a 0.18 M stock solution) was added. The mixture immediately turned dark orange and the resulting solution was diluted with MeCN to a final volume of 2.5 mL, giving a 4.0 mM solution of the starting $[^{57}\text{Fe}^{\text{II}}(\text{N3Py}^{\text{amide}}\text{SR})](\text{BF}_4)_2$ complex.

$[^{57}\text{Fe}^{\text{IV}}(\text{O})(\text{N3Py}^{\text{amide}}\text{SR})](\text{BF}_4)_2$. A solution of $[^{57}\text{Fe}^{\text{II}}(\text{N3Py}^{\text{amide}}\text{SR})](\text{BF}_4)_2$ (0.4 mL, 4 mM) was loaded directly into a Teflon Mössbauer sample cup cooled to $-40 \text{ }^\circ\text{C}$ in an MeCN/dry ice bath using a custom brass sample holder. A stock solution of PhIO was prepared by dissolving PhIO (2.0 mg, 9 μmol) in MeOH (0.38 mL). The PhIO solution (0.1 mL, 1.0 equiv) was injected directly into the sample cup and mixed well by bubbling with Ar. After standing at $-40 \text{ }^\circ\text{C}$ for 45 min, the sample was frozen in $\text{N}_2(\text{l})$ using the custom holder, and stored at 77 K until measurements were performed.

IV. Kinetic Studies

General Methods. Kinetic measurements for the reactions of $[\text{Fe}^{\text{IV}}(\text{O})(\text{N3Py}^{\text{amide}}\text{SR})]^{2+}$ (**2**) with substrates were performed on a Varian Cary 50 spectrophotometer (kinetics mode) in $\text{CH}_3\text{CN}/\text{CH}_3\text{OH}$ at $-40\text{ }^\circ\text{C}$. Reaction rates and pseudo-first-order rate constants (k_{obs}) were measured by the growth of the absorption band at 450 nm corresponding to the return of $[\text{Fe}^{\text{II}}(\text{N3Py}^{\text{amide}}\text{SR})]^{2+}$ (**1**). Monitoring the disappearance of the 750 nm band corresponding to **2** gave the same results. All reactions were performed under pseudo-first-order conditions where the concentration of substrate was at least 20-fold greater than the concentration of iron complex.

Reaction of 2 with PhSMe at $-40\text{ }^\circ\text{C}$. A solution of **1** (5.0 mL, 0.54 mM) in CH_3CN was cooled to $-40\text{ }^\circ\text{C}$ in a flask equipped to accept a submersible UV-vis probe (2 mm path length). A solution of PhIO (0.9 mg, 4.1 μmol) was then added in 0.25 mL of MeOH, and the reaction mixture was stirred at $-40\text{ }^\circ\text{C}$ for 30 min or until the full formation of **2** was observed by UV-vis spectroscopy. A solution of PhSMe in CH_3CN ($1.0 \times 10^{-2} - 5.0 \times 10^{-2}$ M, 0.1 mL total volume) was added, and the change in absorbance at 450 nm was monitored for ~ 500 s. The UV-vis spectral changes for a representative reaction are shown in Figure S7, and reveal two kinetic phases. The first phase shows good isosbestic behavior for the conversion of **2** to **1**, followed by a second phase in which the original isosbestic point at 322 nm is lost. The first kinetic phase was assigned to the reaction $\mathbf{2} + \text{PhSMe} \rightarrow \mathbf{1} + \text{PhS(O)Me}$, and typically corresponded to 60 – 70% reaction completion. These data were easily modeled with a single exponential function as described below. The origin of the second, slower kinetic phase was not determined. A plot of ΔA (450 nm) versus time (Figure S8) for the first phase was fit to the following single exponential function:

$$A_t = (\Delta A)e^{-k_{\text{obs}}t} + A_f \quad (\text{eq 1})$$

where A_t = absorbance at time t ; ΔA = total change in absorbance from $t = 0$ to $t = \text{final}$; A_f = absorbance at final time t (5 half-lives); and k_{obs} = pseudo-first-order rate constant.

The k_{obs} values obtained from the fits to eq 1 were plotted versus [PhSMe] (Figure S9), and found to give a linear relationship. The slope yields the second-order rate constant $k = 4.3 \text{ M}^{-1} \text{ s}^{-1}$ for the reaction between **2** and PhSMe (Figure S9).

Reaction of 2 with 2,4-di-tert-butyl phenol at -40 °C. A solution of **1** in MeCN (4.0 mL, 0.5 mM) was cooled to -40 °C in a flask equipped to accept a submersible UV-vis probe. PhIO (0.54 mg, 2.5 μmol) was added as a solution in 0.1 mL of MeOH and allowed to stir for 30 min until full formation of **2** was observed by UV-vis spectroscopy. A solution of 2,4-di-tert-butyl phenol (1.0 mmol, 500 equiv) in CH_2Cl_2 (700 μL) was added and the growth of the absorbance at 450 nm was monitored for 80 min (Figure S11). Total recovery of **1** was 98% as measured by the absorbance of the final peak at 650 nm ($\epsilon = 6000 \text{ M}^{-1} \text{ cm}^{-1}$). The growth of the absorbance at 450 nm was fit using a single exponential function to give a $k_{\text{obs}} = 4.0 \times 10^{-3} \text{ s}^{-1}$ (Figure S12).

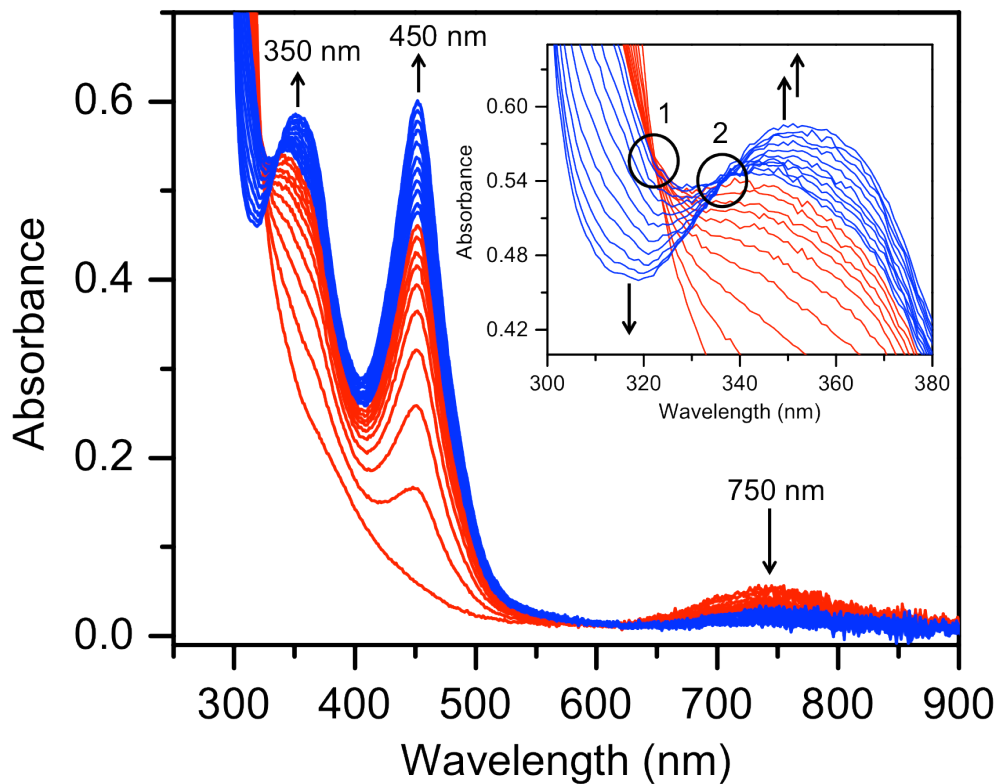


Figure S7. UV-vis spectral changes over 30 min for the reaction of **2** (0.39 mM) with PhSMe (21.6 mM) in CH₃CN/CH₃OH at -40 °C. Red spectra = first kinetic phase, blue spectra = second kinetic phase. Inset: spectral changes for 300 - 380 nm showing the two isosbestic points (circles) for the first kinetic phase (322 nm), and the second kinetic phase (337 nm).

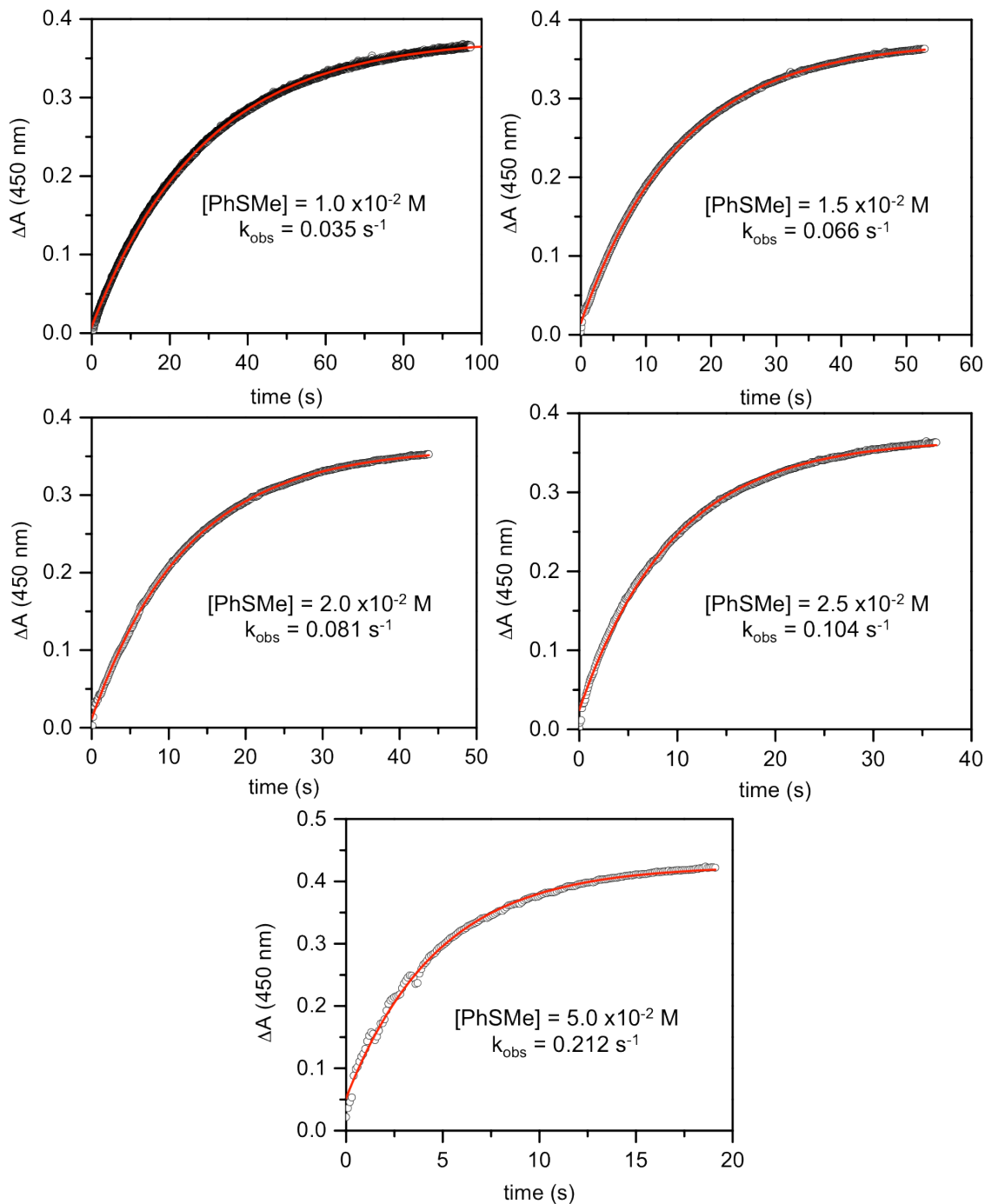


Figure S8. Plots for $\Delta A_{(450\text{ nm})}$ versus time for the reaction of **2** with PhSMe in $\text{CH}_3\text{CN}/\text{CH}_3\text{OH}$ ($[\text{PhSMe}] = 1.0 \times 10^{-2} - 5.0 \times 10^{-2}$ M). Experimental = open circles; best fit = red line.

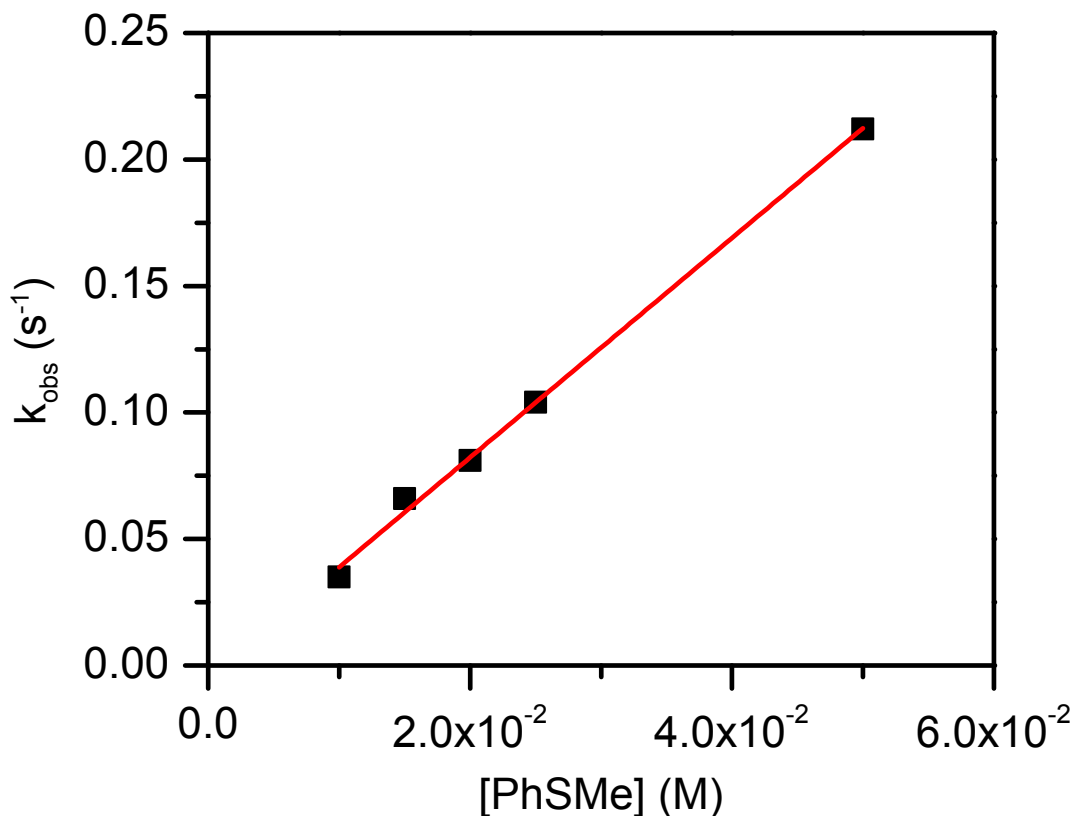


Figure S9. Plot of k_{obs} vs [PhSMe] (squares) and best fit (red line).

V. Yield of PhS(O)Me in the reaction of 2 + PhSMe in $\text{CH}_3\text{CN}/\text{CH}_3\text{OH}$ at -40°C . Compound **1** (1.3 mg, 1.8 μmol) was dissolved in CD_3CN (0.25 mL), and cooled to -40°C in an acetonitrile/dry ice bath. The oxidant, PhIO (0.47 mg, 2.1 μmol), was added as a solution in MeOD (50 μL), and allowed to stand at -40°C for 45 min. The solution lightened in color from orange to yellow. Thioanisole (PhSMe, 10.0 equiv, 2.09 μL) was then added as a solution in CD_3CN (50 μL), and the reaction mixture was allowed to stand at -40°C for 30 min before warming to room temperature. Peaks in the ^1H NMR spectrum corresponding to PhSMe and PhS(O)Me were integrated, showing PhS(O)Me was formed in 80% yield (versus iron).

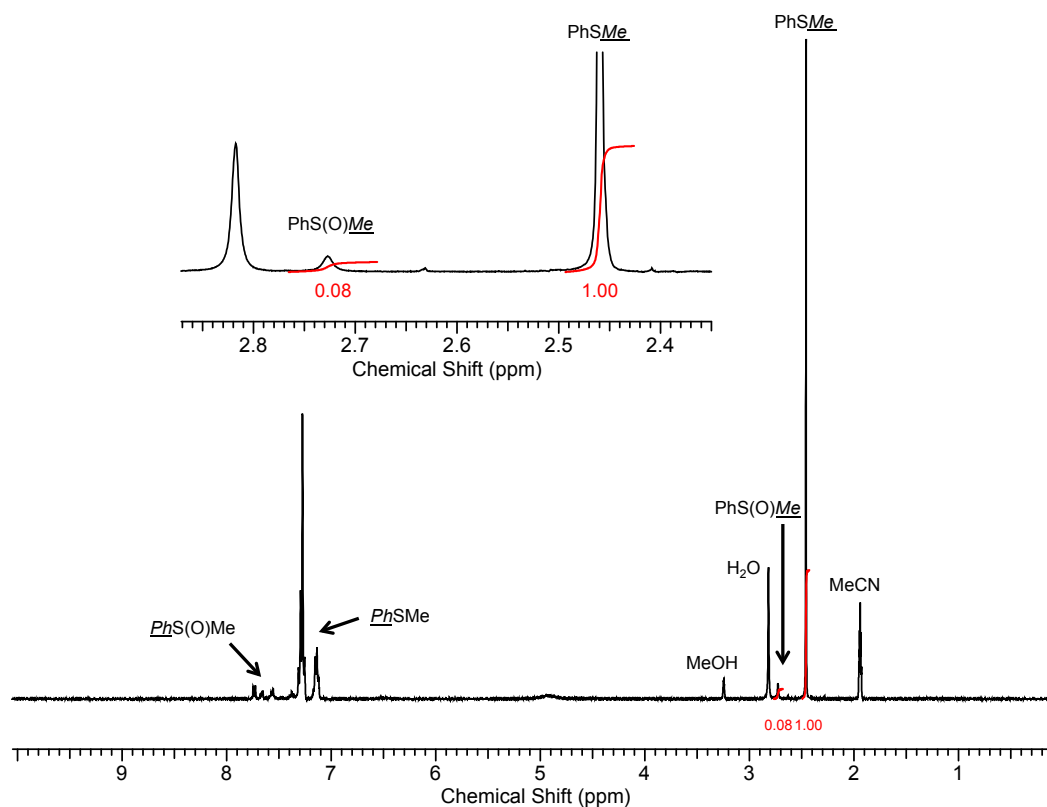


Figure S10. ^1H -NMR spectrum of the reaction of **2** + thioanisole (10 equiv) at $-40\text{ }^\circ\text{C}$, in $\text{CD}_3\text{CN}/\text{CD}_3\text{OD}$, for 30 min. Compound **2** was formed in the sample tube with 1.2 equiv PhIO before PhSMe was added. Phenylmethyl sulfoxide (PhS(O)Me, 2.73 ppm) is formed in 80% yield (versus iron), as compared to the starting material (PhSMe, 2.44 ppm), integrations are shown in red.

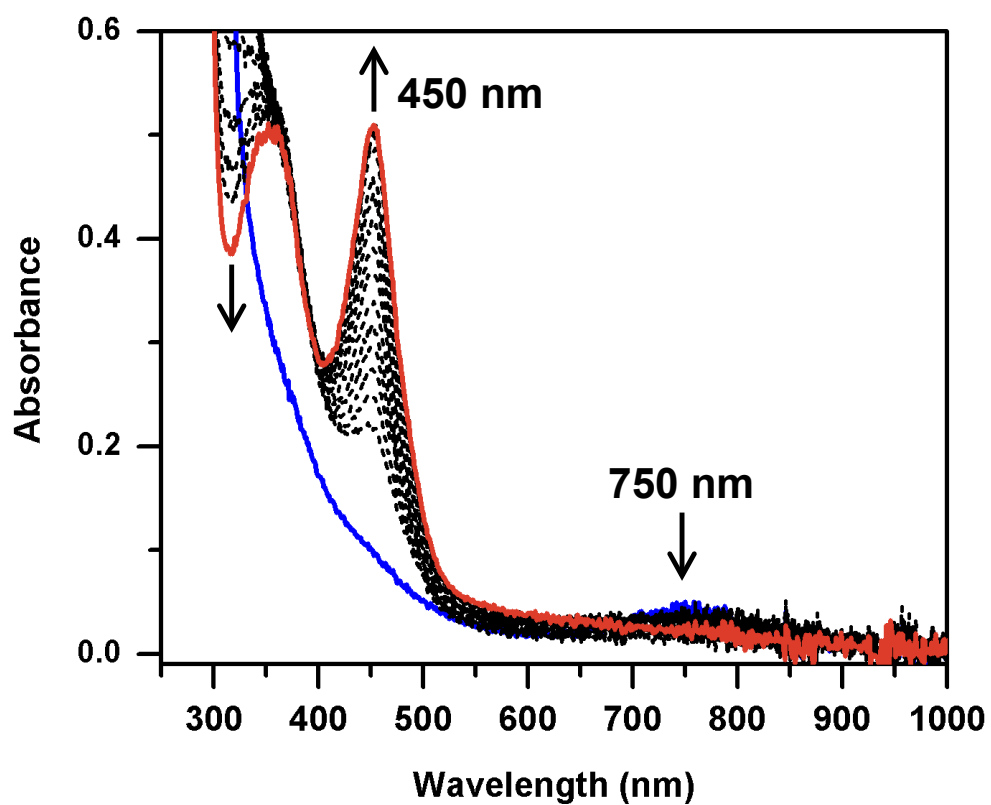


Figure S11. UV-vis spectral changes of **2** + 2,4-di-tert-butyl phenol (500 equiv) over 80 min in $\text{CH}_3\text{CN}/\text{CH}_3\text{OH}$ at $-40\text{ }^\circ\text{C}$.

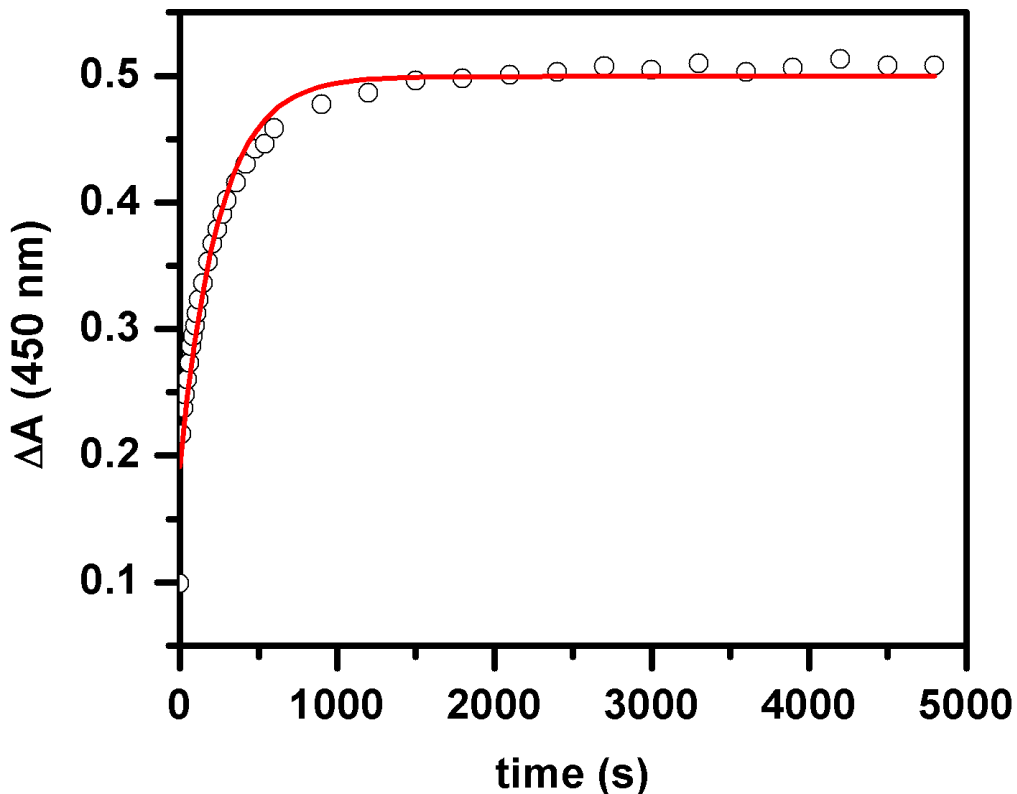


Figure S12. Plot of the change in absorbance at 450 nm for the reaction of **2** + 2,4-di-tert-butyl phenol (500 equiv) in CH₃CN/CH₃OH at -40 °C. Experimental = Open circles, best fit = red line.

VI. Catalytic oxidations. Compound **1** (1.0 mg, 1.4 μ mol) was dissolved in 0.3 mL CD₃CN, and placed in an NMR tube. Thioanisole (100 equiv, 16 μ L) was added as a solution in CD₃CN (100 μ L), and then the oxidant PhIO (50 equiv, 15.1 mg) was added as a solution in MeOD (250 μ L). Immediately upon addition of the oxidant, there is a transient color change to yellow, followed by a darkening toward orange. After 30 min, the solution is pale yellow in color, likely due to catalyst decomposition. The reaction mixture was allowed to stand for a total of 2 h. Comparison of the ¹H NMR peaks for PhSMe and PhS(O)Me reveal PhS(O)Me was produced in 85% yield as compared to oxidant, which corresponds to \sim 43 turnovers.

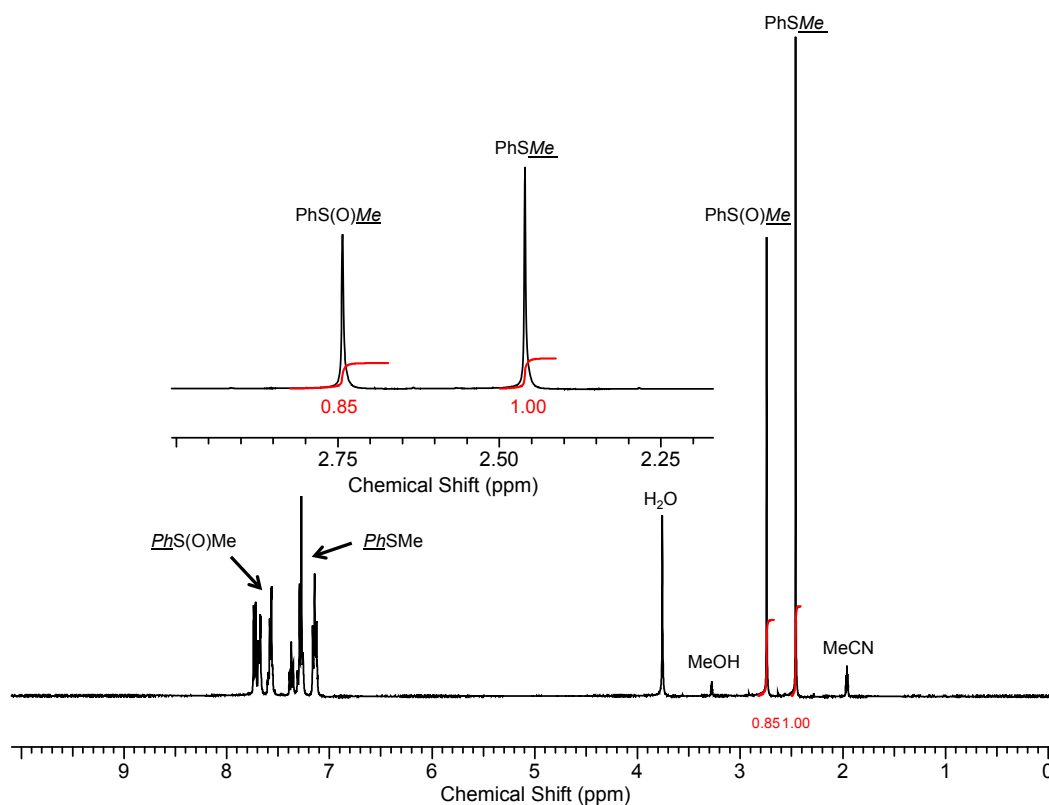


Figure S13. ^1H NMR spectrum of the catalytic oxidation of thioanisole with **1** as catalyst and PhIO as oxidant in $\text{CD}_3\text{CN}/\text{CD}_3\text{OD}$ at 25 °C (PhSMe : PhIO : **1** = 100 : 50 : 1). Phenylmethyl sulfoxide (PhS(O)Me, 2.73 ppm) is formed in 85% yield (versus oxidant), as compared to the thioanisole (PhSMe, 2.44 ppm), integrations are shown in red.

VII. Density Functional Calculations

The optimized structures are presented in Figures S14 and S15, with relevant bond distances and angles compared with the data from the X-ray structures available in Table S1. The bond distances compare favorably except for the Fe-S distances, which are known to be over-estimated by DFT calculations.¹⁵ Mössbauer parameters calculated by using the optimized structures are compared in Table S3. The Mössbauer parameters of the $^1\text{Fe}^{\text{II}}$ complex **1** are predicted with a calculated isomer shift within 0.08 mm s^{-1} and the quadrupole splitting within 0.06 mm s^{-1} of experiment. The Mössbauer parameters for the $\text{Fe}^{\text{IV}}(\text{O})$ complex **2** were calculated with the optimized structure obtained from the higher-level calculations described in the Computational Methods section. The isomer shift of $^3\text{Fe}^{\text{IV}}$ is underestimated by only 0.01 mm s^{-1} by DFT, while the quadrupole splitting is underestimated by 0.25 mm s^{-1} . These calculated parameters are a reasonable fit to the experimental data, and are well within the error seen in the literature.^{16,14}

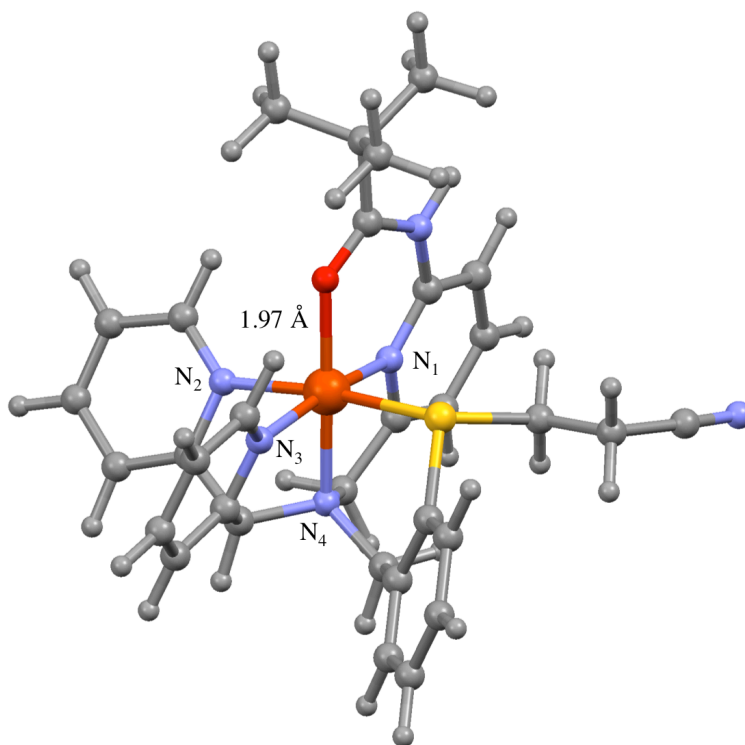


Figure S14. DFT optimized structures of $^1[\text{Fe}^{\text{II}}(\text{N3Py}^{\text{amide}}\text{SR})]^{2+}$ using the B3LYP/6-31G(d) functional on all atoms.

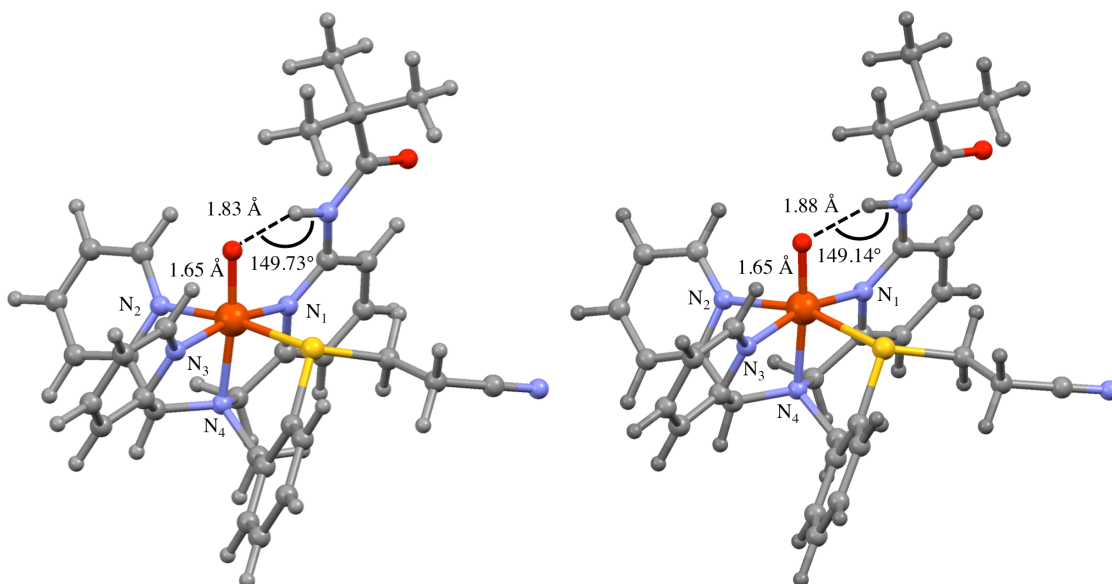


Figure S15. DFT optimized structure of $[\text{Fe}^{\text{IV}}(\text{O})(\text{N3Py}^{\text{amide}}\text{SR})]^{2+}$ in the triplet (left) and quintet (right) spin states. Geometries calculated with LANLDZ on the iron and 6-31G on the rest of the atoms, including the auxiliary basis sets def2-SVP/J and def2-SVP/K for the RIJCOSX approximation, with DFT at the unrestricted hybrid density functional level B3LYP.

Table S1. Comparison of selected bond distances (Å) and angles (°) for the X-ray crystal structure of **1**, and those obtained from DFT calculations for the Fe^{II} (**1**), $\text{ls-Fe}^{\text{IV}}(\text{O})$ (**3**) and $\text{hs-Fe}^{\text{IV}}(\text{O})$ (**5**) complexes.

	1 (X-ray)	$^1\text{Fe}^{\text{II}}$ ^a	$^3\text{Fe}^{\text{IV}}$ ^b	$^5\text{Fe}^{\text{IV}}$ ^b
Fe-O	1.95	1.97	1.65	1.65
Fe-N ₄	1.98	2.02	2.09	2.08
Fe-N ₃	1.92	1.99	1.99	2.07
Fe-N ₂	1.96	2.01	1.98	2.19
Fe-N ₁	1.97	1.95	2.03	2.05
Fe-S	2.29	2.41	2.45	2.75
C=O	1.25	1.25	N/A	N/A
Fe=O---H	N/A	N/A	1.83	1.88
O---H-N	N/A	N/A	149.73°	149.14°

^a 6-31G(d) basis set. ^b LANLDZ on the iron and 6-31G basis set on the rest of the atoms, including the auxiliary basis sets def2-SVP/J and def2-SVP/K for the RIJCOSX approximation. See Computational Methods for complete details.

Table S2. Calculated absolute and relative energies of the ls (S = 1) and hs (S = 2) forms of **2**.

	E ^a (Eh)	ΔE (kcal mol ⁻¹)
³ [Fe ^{IV} (O)(N3Py ^{amide} SR)] ²⁺	-2238.635984	0
⁵ [Fe ^{IV} (O)(N3Py ^{amide} SR)] ²⁺	-2238.632402	+2.3

^a Sum of electronic energy, zero-point energy, and thermal energy in atomic energy units.

Table S3. Comparison of the experimental (exp.) and calculated (calc.) Mössbauer parameters for **1** and **2**.

	¹ [Fe ^{II} (N3Py ^{amide} SR)] ²⁺		³ Fe ^{IV}	⁵ Fe ^{IV}	2
	calc.	exp.	calc.		exp.
δ (mm s ⁻¹)	0.39	0.47	0.03	0.12	0.04
ΔE _Q (mm s ⁻¹)	0.82	0.77	0.55	-1.26	0.80

Table S4. Comparison of low-spin and high-spin Mössbauer parameters for selected Fe^{IV}(O) complexes.

	δ (mm s ⁻¹)	ΔE _Q (mm s ⁻¹)	Citation
Low-Spin (S = 1)			
[Fe ^{IV} (O)(N4Py)] ²⁺	-0.04	0.93	17
[Fe ^{IV} (O)(TPA)(NCCH ₃)] ²⁺	0.01	0.92	18
[Fe ^{IV} (O)(cyclam-CH ₂ CO ₂)] ⁺	0.01	1.37	19
[Fe ^{IV} (O)(N3Py ^{amide} SR)] ²⁺	0.04	0.80	This work
[Fe ^{IV} (O)(TMC)(NCCH ₃)] ²⁺	0.17	1.24	20
[Fe ^{IV} (O)(^{Me,H} Pytacn)] ²⁺	0.05	0.73	21
[Fe ^{IV} (O)(BisPi1)] ²⁺	0.02	0.69	22
[Fe ^{IV} (O)(TBC)(NCCH ₃)] ²⁺	0.22	0.97	23
High-Spin (S = 2)			
[Fe ^{IV} H3buea(O)] ⁻	0.02	0.43	24
[Fe ^{IV} (O)(TMG ₃ tren)] ²⁺	0.09	-0.29	25
[Fe ^{IV} (O)(tpa ^{ph})] ⁻	0.09	0.51	26
CytC3•Fe(II)•RKG•L-Aba-S-CytC2•Br ⁻ Species 1	0.23	0.81	27
TyrH ¹	0.25	-1.27	28
Prolyl-4-Hydroxylase	0.30	-0.82	29
TauD	0.31	0.88	30
CytC3•Fe(II)•RKG•L-Aba-S-CytC2•Br ⁻ Species 2	0.31	1.06	27
[Fe ^{IV} (O)(H ₂ O) ₅] ²⁺	0.38	-0.33	31

Cartesian coordinates for $^1\text{Fe}^{\text{II}}$ (1).

26	-0.09757	-0.611783	0.371692
8	-1.030409	-1.01577	2.063982
16	-0.597811	1.722522	0.700252
7	0.799787	-0.328836	-1.414015
6	-2.012969	2.387765	-0.292597
1	-2.864199	1.758374	-0.016265
6	-2.356173	3.86748	-0.019712
1	-2.523649	4.031362	1.052636
1	-1.526626	4.519099	-0.319723
6	-3.564418	4.187235	-0.784227
7	-4.526453	4.335739	-1.418168
6	0.82058	2.617649	0.050525
6	1.262357	3.741645	0.756208
6	1.510173	2.177629	-1.098822
6	2.367159	4.470261	0.305282
1	0.73333	4.05074	1.653055
6	2.621055	2.915867	-1.526207
6	3.045962	4.056189	-0.839088
1	2.687772	5.356262	0.845433
1	3.148691	2.615707	-2.429044
1	3.899308	4.619192	-1.205386
6	0.997011	1.063469	-1.982849
1	0.007326	1.340443	-2.362417
6	-1.504166	-1.095353	-1.994576
6	-4.057448	-1.361198	-1.02202
6	-2.547397	-1.265865	-2.89309
1	-5.056991	-1.482614	-0.612632
1	-2.355934	-1.311063	-3.961064
6	-2.954834	-1.170015	-0.174343
6	-3.850598	-1.394688	-2.39432
1	-4.689858	-1.530509	-3.070564
7	-1.706849	-1.017145	-0.650536
7	0.624127	-2.474574	0.133813
6	0.22015	-3.654221	0.637542
6	1.720766	-2.457532	-0.664013
1	-0.647367	-3.621403	1.287423
6	2.429392	-3.606959	-0.994035
6	1.999552	-4.83135	-0.470144
1	3.29897	-3.553723	-1.643213
1	2.531159	-5.748415	-0.70848
7	1.698039	-0.217393	1.140915
6	2.067105	0.186301	2.368983
6	2.656544	-0.406372	0.202335
1	1.260353	0.318781	3.082438
6	4.005364	-0.192821	0.458146
6	4.3849	0.226535	1.737029
1	4.747985	-0.35475	-0.318015
1	5.432303	0.396364	1.970523
6	0.880598	-4.851363	0.362565

6	3.400298	0.411629	2.707842
1	-1.832114	2.234043	-1.360739
6	-0.044545	-1.079885	-2.41359
6	2.092159	-1.036612	-1.067664
7	-3.161595	-1.140667	1.22048
1	0.521078	-5.779747	0.795062
1	3.657828	0.721995	3.715628
1	0.072538	-0.657281	-3.418318
1	0.304417	-2.114488	-2.472722
1	2.816676	-1.019066	-1.893677
1	1.650907	0.974211	-2.861524
6	-2.257066	-1.141432	2.259603
6	-2.805677	-1.336511	3.68251
1	-4.126769	-1.236889	1.512391
6	-2.277757	-0.173885	4.560138
1	-1.18596	-0.133864	4.550048
1	-2.66653	0.796156	4.231766
1	-2.598035	-0.322201	5.595621
6	-2.232658	-2.68531	4.199377
1	-2.553348	-2.846588	5.232999
1	-2.599884	-3.537926	3.614968
1	-1.139563	-2.68599	4.184352
6	-4.348173	-1.376234	3.751128
1	-4.663471	-1.48971	4.792338
1	-4.81833	-0.446655	3.402475
1	-4.782556	-2.237749	3.224349

Cartesian coordinates for ${}^3\text{Fe}^{\text{IV}}(\text{O})$ (32).

26	0.052835	-0.020757	-0.045694
16	-1.136154	2.089055	0.324624
6	-2.782267	2.239344	-0.658584
6	-3.428848	3.623213	-0.447736
6	-4.704308	3.674496	-1.163590
7	-5.717883	3.679503	-1.750349
1	-3.600468	3.811558	0.619013
1	-2.771958	4.418568	-0.819973
1	-3.399958	1.442557	-0.240233
1	-2.585274	2.036450	-1.712220
6	-0.035580	3.389114	-0.428318
6	0.073874	4.595445	0.271784
6	0.913675	5.608275	-0.213121
6	1.657354	5.394749	-1.376820
6	1.555026	4.176016	-2.057741
6	0.706222	3.151191	-1.602039
6	0.513694	1.936203	-2.479202
7	0.782346	0.542222	-1.920129
6	0.169830	-0.440271	-2.898917
6	-1.216461	-0.838929	-2.462935
7	-1.468593	-0.850782	-1.107396
6	-2.680020	-1.343609	-0.657267

7	-2.897838	-1.388264	0.710557
6	-4.090648	-1.790439	1.369974
8	-5.110199	-2.093246	0.728781
6	-4.073215	-1.871884	2.904080
6	-5.357541	-1.161687	3.410646
1	-5.326140	-0.084075	3.205584
1	-6.243542	-1.577144	2.926229
1	-5.448998	-1.303021	4.492866
6	-4.152057	-3.384559	3.267329
1	-4.204954	-3.494863	4.355892
1	-5.042770	-3.841165	2.828319
1	-3.269212	-3.930463	2.911621
6	-2.824386	-1.247040	3.559219
1	-2.714143	-0.182071	3.315322
1	-2.921705	-1.321312	4.647338
1	-1.898498	-1.767900	3.287317
1	-2.104057	-1.139702	1.297861
6	-3.654495	-1.783620	-1.589903
6	-3.389068	-1.730494	-2.946984
6	-2.149713	-1.251348	-3.399395
1	-1.912745	-1.216185	-4.456688
1	-4.139591	-2.063651	-3.654147
1	-4.595259	-2.145405	-1.204116
1	0.149547	-0.003133	-3.902119
1	0.801245	-1.329187	-2.959094
6	2.250666	0.246070	-1.633339
6	2.295198	-1.224546	-1.230552
7	1.260913	-1.547803	-0.404297
6	1.143987	-2.792012	0.107167
6	2.078488	-3.780497	-0.213832
6	3.143171	-3.465631	-1.065841
6	3.258523	-2.163974	-1.582786
1	4.073065	-1.898342	-2.246482
1	3.875524	-4.220236	-1.329461
1	1.967530	-4.773771	0.203197
1	0.309673	-2.971003	0.771669
6	2.643520	1.016237	-0.383109
7	1.696210	0.914750	0.589422
6	1.935076	1.378337	1.836897
6	3.158975	1.978622	2.148879
6	4.132297	2.108010	1.152362
6	3.873120	1.618284	-0.138057
1	4.616461	1.694953	-0.923476
1	5.084069	2.575848	1.376999
1	3.344343	2.333710	3.155121
1	1.145914	1.238857	2.564773
1	2.895934	0.469174	-2.488838
1	-0.526613	1.895623	-2.818032
1	1.133415	2.044397	-3.377956
1	2.121354	4.028634	-2.972563
1	2.307416	6.173056	-1.760573

1	0.981769	6.550706	0.318236
1	-0.490537	4.748486	1.184931
8	-0.371158	-0.564297	1.456453

Cartesian coordinates of ${}^5\text{Fe}^{\text{IV}}(\text{O})$ (52).

26	0.004018	-0.200749	-0.007543
16	-1.216514	2.231970	0.389987
6	-2.899526	2.562436	-0.484983
6	-3.401798	3.994737	-0.214001
6	-4.698625	4.192546	-0.865769
7	-5.732052	4.314677	-1.403887
1	-3.501805	4.169222	0.863803
1	-2.688000	4.731848	-0.599899
1	-3.564380	1.815400	-0.046686
1	-2.785315	2.369215	-1.553050
6	-0.034971	3.393472	-0.455685
6	0.239396	4.609059	0.181015
6	1.169337	5.498521	-0.376961
6	1.822624	5.165391	-1.566655
6	1.550042	3.944077	-2.192074
6	0.626056	3.032816	-1.648283
6	0.303856	1.783328	-2.431028
7	0.711341	0.411583	-1.870148
6	0.148104	-0.617077	-2.834765
6	-1.257754	-0.994205	-2.443263
7	-1.544759	-0.996042	-1.088659
6	-2.780027	-1.457243	-0.659949
7	-3.023628	-1.491547	0.698946
6	-4.239214	-1.867675	1.339895
8	-5.243014	-2.175427	0.678155
6	-4.263064	-1.905880	2.875087
6	-5.539471	-1.145524	3.327737
1	-5.474454	-0.076193	3.091202
1	-6.425237	-1.553103	2.836854
1	-5.657839	-1.250600	4.411093
6	-4.397186	-3.404560	3.279941
1	-4.499197	-3.477594	4.367906
1	-5.281055	-3.850742	2.817889
1	-3.515215	-3.983343	2.980114
6	-3.015000	-1.293494	3.543964
1	-2.881993	-0.234940	3.284443
1	-3.135338	-1.345881	4.630749
1	-2.094428	-1.838160	3.301868
1	-2.239734	-1.254047	1.302675
6	-3.744501	-1.872189	-1.614864
6	-3.442535	-1.833270	-2.963928
6	-2.178121	-1.391579	-3.394171
1	-1.920596	-1.372264	-4.446566
1	-4.184437	-2.149827	-3.687411

1	-4.702612	-2.210086	-1.251308
1	0.172183	-0.220384	-3.854826
1	0.781646	-1.504583	-2.819521
6	2.210373	0.259651	-1.631180
6	2.469086	-1.204733	-1.281806
7	1.528191	-1.709672	-0.437217
6	1.655953	-2.958086	0.062588
6	2.750522	-3.758902	-0.283490
6	3.713662	-3.253861	-1.163854
6	3.574595	-1.951538	-1.674902
1	4.313003	-1.540399	-2.353640
1	4.564338	-3.860679	-1.451591
1	2.843004	-4.754014	0.132827
1	0.879528	-3.294954	0.738161
6	2.565546	1.042039	-0.373089
7	1.654528	0.867839	0.625429
6	1.897307	1.335038	1.872956
6	3.084256	2.013828	2.160732
6	4.017280	2.219128	1.137959
6	3.757427	1.724960	-0.150378
1	4.471717	1.865914	-0.953174
1	4.940240	2.750109	1.340598
1	3.273037	2.373266	3.164540
1	1.134905	1.143497	2.617963
1	2.792874	0.583732	-2.499840
1	-0.773238	1.695815	-2.596242
1	0.778053	1.860206	-3.417341
1	2.044636	3.704275	-3.128706
1	2.531403	5.854155	-2.012445
1	1.374277	6.443061	0.114019
1	-0.267586	4.861828	1.105678
8	-0.438717	-0.740200	1.484566

VIII. References

- (1) Blackmond, D. G.; Hodnett, N. S.; Lloyd-Jones, G. C. *J. Am. Chem. Soc.* **2006**, *128*, 7450.
- (2) Thapper, A.; Behrens, A.; Fryxelius, J.; Johansson, M. H.; Prestopino, F.; Czaun, M.; Rehder, D.; Nordlander, E. *Dalton Trans.* **2005**, 3566.
- (3) Najera, C.; Gil-Molto, J.; Karlstrom, S. *Adv. Synth. Catal.* **2004**, *346*, 1798.
- (4) Sahu, S.; Widger, L. R.; Quesne, M. G.; de Visser, S. P.; Matsumura, H.; Möenne-Loccoz, P.; Siegler, M. A.; Goldberg, D. P. *J. Am. Chem. Soc.* **2013**, *135*, 10590.
- (5) Frisch, M.J.; et al. *Gaussian 09*, Revision A.1; Gaussian, Inc.: Wallingford, CT, 2009.
- (6) Neese, F. *Wiley Interdiscip. Rev.: Comput. Mol. Sci.* **2012**, *2*, 73.
- (7) Francl, M. M.; Pietro, W. J.; Hehre, W. J.; Binkley, J. S.; Gordon, M. S.; Defrees, D. J.; Pople, J. A. *J. Chem. Phys.* **1982**, *77*, 3654.
- (8) Hehre, W. J.; Ditchfie.R; Pople, J. A. *J. Chem. Phys.* **1972**, *56*, 2257.

- (9) Rassolov, V. A.; Pople, J. A.; Ratner, M. A.; Windus, T. L. *J. Chem. Phys.* **1998**, *109*, 1223.
- (10) Neese, F.; Wennmohs, F.; Hansen, A.; Becker, U. *Chem. Phys.* **2009**, *356*, 98.
- (11) Kendall, R. A.; Früchtl, H. A. *Theor. Chem. Acc.* **1997**, *97*, 158.
- (12) Sinnecker, S.; Slep, L. D.; Bill, E.; Neese, F. *Inorg. Chem.* **2005**, *44*, 2245.
- (13) Schafer, A.; Horn, H.; Ahlrichs, R. *J. Chem. Phys.* **1992**, *97*, 2571.
- (14) Römelt, M.; Ye, S.; Neese, F. *Inorg. Chem.* **2008**, *48*, 784.
- (15) Kumar, D.; Thiel, W.; de Visser, S. P. *J. Am. Chem. Soc.* **2011**, *133*, 3869.
- (16) Neese, F. *Coord. Chem. Rev.* **2009**, *253*, 526.
- (17) Kaizer, J.; Klinker, E. J.; Oh, N. Y.; Rohde, J. U.; Song, W. J.; Stubna, A.; Kim, J.; Münck, E.; Nam, W.; Que, L., Jr. *J. Am. Chem. Soc.* **2004**, *126*, 472.
- (18) Lim, M. H.; Rohde, J. U.; Stubna, A.; Bukowski, M. R.; Costas, M.; Ho, R. Y. N.; Münck, E.; Nam, W.; Que, L., Jr. *Proc. Natl. Acad. Sci. U. S. A.* **2003**, *100*, 3665.
- (19) Grapperhaus, C. A.; Mienert, B.; Bill, E.; Weyhermuller, T.; Wieghardt, K. *Inorg. Chem.* **2000**, *39*, 5306.
- (20) Rohde, J. U.; In, J. H.; Lim, M. H.; Brennessel, W. W.; Bukowski, M. R.; Stubna, A.; Münck, E.; Nam, W.; Que, L., Jr. *Science* **2003**, *299*, 1037.
- (21) Company, A.; Prat, I.; Frisch, J. R.; Mas-Balleste, R.; Guell, M.; Juhasz, G.; Ribas, X.; Münck, E.; Luis, J. M.; Que, L., Jr.; Costas, M. *Chem. – Eur. J.* **2011**, *17*, 1622.
- (22) Bautz, J.; Bukowski, M. R.; Kerscher, M.; Stubna, A.; Comba, P.; Lienke, A.; Münck, E.; Que, L., Jr. *Angew. Chem. Int. Ed.* **2006**, *45*, 5681.
- (23) Wilson, S. A.; Chen, J.; Hong, S.; Lee, Y. M.; Clemancey, M.; Garcia-Serres, R.; Nomura, T.; Ogura, T.; Latour, J. M.; Hedman, B.; Hodgson, K. O.; Nam, W.; Solomon, E. I. *J. Am. Chem. Soc.* **2012**, *134*, 11791.
- (24) Lacy, D. C.; Gupta, R.; Stone, K. L.; Greaves, J.; Ziller, J. W.; Hendrich, M. P.; Borovik, A. S. *J. Am. Chem. Soc.* **2010**, *132*, 12188.
- (25) England, J.; Martinho, M.; Farquhar, E. R.; Frisch, J. R.; Bominaar, E. L.; Münck, E.; Que, L., Jr. *Angew. Chem. Int. Ed.* **2009**, *48*, 3622.
- (26) Bigi, J. P.; Harman, W. H.; Lassalle-Kaiser, B.; Robles, D. M.; Stich, T. A.; Yano, J.; Britt, R. D.; Chang, C. J. *J. Am. Chem. Soc.* **2012**, *134*, 1536.
- (27) Fujimori, D. G.; Barr, E. W.; Matthews, M. L.; Koch, G. M.; Yonce, J. R.; Walsh, C. T.; Bollinger, J. M., Jr.; Krebs, C.; Riggs-Gelasco, P. J. *J. Am. Chem. Soc.* **2007**, *129*, 13408.
- (28) Eser, B. E.; Barr, E. W.; Frantorn, P. A.; Saleh, L.; Bollinger, J. M., Jr.; Krebs, C.; Fitzpatrick, P. F. *J. Am. Chem. Soc.* **2007**, *129*, 11334.
- (29) Hoffart, L. M.; Barr, E. W.; Guyer, R. B.; Bollinger, J. M., Jr.; Krebs, C. *Proc. Natl. Acad. Sci. U. S. A.* **2006**, *103*, 14738.
- (30) Krebs, C.; Price, J. C.; Baldwin, J.; Saleh, L.; Green, M. T.; Bollinger, J. M., Jr. *Inorg. Chem.* **2005**, *44*, 742.
- (31) Pestovsky, O.; Stoian, S.; Bominaar, E. L.; Shan, X. P.; Münck, E.; Que, L., Jr.; Bakac, A. *Angew. Chem. Int. Ed.* **2005**, *44*, 6871.